Open access • Posted Content • DOI:10.1101/856948

Rough and smooth variant Mycobacterium abscessus infections are differentially controlled by host immunity during chronic infection — Source link

Elinor Hortle, Julia Y Kam, E. Krogman, S. E. Warner ...+11 more authors

Institutions: University of Sydney, University of New South Wales, Victor Chang Cardiac Research Institute, Centre national de la recherche scientifique ...+1 more institutions

Published on: 29 Nov 2019 - bioRxiv (Cold Spring Harbor Laboratory)

Topics: Mycobacterium abscessus, Chronic infection, Acquired immune system, Immunity and Immune system

Rough and smooth variant *Mycobacterium abscessus* infections are differentially controlled by host immunity during chronic infection

Elinor Hortle[1,2]*, Julia Y Kam[1]*, Elizabeth Krogman[1]*, Sherridan E Warner[1,2]*, Kaiming Luo[1], Tina Cheng[1], Pradeep Manuneedhi Cholan[1], Kazu Kikuchi[3,4], James A Triccas[2], Warwick J Britton[1,2], Matt D Johansen[5], Laurent Kremer[5,6], Stefan H Oehlers[1,2#]

1 Tuberculosis Research Program at the Centenary Institute, The University of Sydney, Camperdown NSW Australia

2 The University of Sydney, Faculty of Medicine and Health & Marie Bashir Institute, Camperdown NSW Australia

3 Developmental and Stem Cell Biology Division, Victor Chang Cardiac Research Institute, Darlinghurst, NSW Australia

4 St. Vincent's Clinical School, University of New South Wales, Kensington, NSW 2052, Australia

5 Centre National de la Recherche Scientifique UMR 9004, Institut de Recherche en Infectiologie de Montpellier (IRIM), Université de Montpellier, 1919 Route de Mende, 34293, Montpellier, France.

6 INSERM, IRIM, 34293 Montpellier, France.

*These authors contributed equally and are listed in alphabetical order.

[#] Corresponding author: Dr Stefan Oehlers, stefan.oehlers@sydney.edu.au

Author contributions

EH, JK, & EK: preliminary experiments; SW, KL, & TC: CFU recovery assays; PMC: histological analysis; KK: provided reagents; JAT & WJB: supervision of study; MDJ: conceived study, supervision of study, wrote manuscript; LK: conceived study, provided reagents, supervision of study, wrote manuscript; SHO: conceived study, performed all experiments, supervision of study, wrote manuscript.

Keywords: non-tuberculous mycobacterium, rapid-growing mycobacteria, animal model, zebrafish, glycopeptidolipids

Abstract

Infections caused by *Mycobacterium abscessus* are increasing in prevalence within patient groups with respiratory comorbidities. Initial colonisation by the smooth colony *M. abscessus* (S) can be followed by an irreversible genetic switch into a highly inflammatory rough colony *M. abscessus* (R), often associated with a decline in pulmonary function. Our understanding of the role of adaptive immunity in *M. abscessus* pathogenesis is largely unknown. Here, we have used intraperitoneal infection of adult zebrafish to model *M. abscessus* pathogenesis in the context of fully functioning host immunity. We find infection with the R variant penetrates host organs causing an inflammatory immune response leading to necrotic granuloma formation within 2 weeks. The R bacilli are targeted by T cell-mediated immunity and burden is constrained. Strikingly, the S variant colonises host internal surfaces at high loads and is met with a robust innate immune response but little T cell-mediated immunity. Invasive granuloma formation is delayed in S variant infection compared to R variant infection upon which T cell-mediated immunity is required to control infection. In mixed infections, the S variant outcompetes the R variant. We also find the R variant activates host immunity to the detriment of S variant *M. abscessus* in mixed infections. These findings demonstrate the applicability of the adult zebrafish to model persistent *M. abscessus* infection and provide insight into the immunopathogenesis of chronic *M. abscessus* infection.

Introduction

Mycobacterium abscessus is an increasingly recognized human pathogen responsible for a wide array of clinical manifestations including muco-cutaneous infections, disseminated or chronic pulmonary diseases (1). The latter is mostly encountered in patients with underlying lung disorders, such as bronchiectasis or cystic fibrosis (CF). Irrespective of being a rapid-growing mycobacteria (RGM), *M. abscessus* displays many pathophysiological traits with slow-growing mycobacteria (SGM), such as *Mycobacterium tuberculosis*. These include the capacity to persist silently within granulomatous structures and to produce pulmonary caseous lesions (2, 3). In addition, *M. abscessus* is notorious for being one of the most-drug resistant mycobacterial species, characterized by a wide panel of acquired and innate drug resistance mechanisms against nearly all anti-tubercular drugs, as well as many different classes of antibiotics (1, 4). Consequently, this explains the complexity and duration of the treatments and the high level of therapeutic failure (5).

M. abscessus exists either as smooth (S) or a rough (R) colony morphotype variants associated with distinct clinical outcomes (6). Previous epidemiological studies have highlighted the association of the R variant, persisting for many years in the infected host, with a rapid decline in pulmonary functions (7-9). It is well established that these morphological differences between S and R variants are dependent on the presence or absence of surface-exposed glycopeptidolipids (GPL), respectively (6, 10-12). However, our knowledge of the pathophysiological characteristics and

interactions between R or S variants with the host immune cells remains largely incomplete and is hampered by the lack of animal models that are permissive to persistent *M. abscessus* infection (13).

Intravenous injection or aerosol administration of *M. abscessus* in immunocompetent BALB/c mice fails to establish a persistent infection, typified by a rapid clearance of the bacilli from the liver, spleen and lungs within 4 weeks (14). Immunosuppression is required to produce a progressive high level of infection with *M. abscessus* in mice, as shown in nude, SCID (severe combined immunodeficiency), interferon-gamma (GKO) and granulocyte-macrophage colony-stimulating factor (GM-CSF) knock-out mice (15).

The contribution of B and T cells in the control of *M. abscessus* infection has been studied in C57BL/6 mice with $Rag2^{-/-}$, $Cd3e^{-/-}$ and $\mu MT^{-/-}$ knockouts (16). These studies indicated that infection control was primarily T cell dependent in the spleen, and both B and T cell dependent in the liver. In addition, IFNg-receptor KO mice ($ifngr1^{-/-}$) were significantly impaired in their control of *M. abscessus* both in the spleen and in the liver, with markedly different granulomas and more pronounced in $TNF^{-/-}$ mice (16). This points to the central role of T cell immunity, IFNg and TNF for the control of *M. abscessus* in C57BL/6 mice, similarly to the control of *M. tuberculosis* infection.

In recent years, alternative non-mammalian models, such as Drosophila (17), Galleria larvae (18), and zebrafish embryos (13) have been developed to study the chronology and pathology of *M. abscessus* infection and for *in vivo* therapeutic assessment of drugs active against *M. abscessus*. In particular, zebrafish embryos have delivered important insights into the pathogenesis of *M. abscessus* and the participation of innate immunity in controlling infection (10, 19). The optical transparency of zebrafish embryos has been used to visualise the formation of large extracellular cords by the R form *in vivo*, representing a mechanism of immune subversion by preventing phagocytic destruction and highlighting the importance bacterial virulence factors such as the dehydratase MAB_4780 and the $MmpL8_{MAB}$ lipid transporter (10, 20, 21). Other studies in zebrafish embryos have demonstrated the contribution of host TNF signalling and IL8-mediated neutrophil recruitment for protective granulomatous immunity against *M. abscessus* (19), and the link between dysfunctional CFTR and vulnerability to *M. abscessus* infection via the macrophage oxidative response (22).

Adult zebrafish models have been well-described for the study of mycobacterial pathogenesis by *Mycobacterium marinum*, used as a surrogate for the closely related *M. tuberculosis*, and the human pathogen *Mycobacterium leprae* (23-26). Encompassing a fully functional immune system, previous studies in adult zebrafish with pathogenic mycobacteria such as *M. marinum* have unravelled the interplay between innate and adaptive immunity in mycobacterial granuloma formation and function.

Herein, we addressed whether adult zebrafish may be a useful host to analyse and compare the chronology of infection with *M. abscessus* S and R variants and to study the contribution of the T cell-mediated immunity and granulomatous response in *M. abscessus* infection.

Results

Adult zebrafish can be chronically infected with *M. abscessus.*

We attempted to infect adult zebrafish with approximately 10^5 CFU per animal with the rough (R) and smooth (S) variants of the reference strain CIP104536^T, scaled for the smaller size of zebrafish from 10^6-10^7 used in mouse intravenous infections (14-16). To determine if *M. abscessus* produces a persistent infection in adult zebrafish, we performed CFU recovery on animals across 28 days of infection (Figure 1A). Variation in the initial inoculum ranging from 10^4-10^6 did not appear to impact the course of infection burden with stable burden of the R variant within a 1-log window either side of the inoculation dose to 28 days post infection (dpi) and progressive growth of the S variant to approximate 1-log above the inoculation dose at 28 dpi in all three experiments.

Normalising burdens across three independent experiments per *M. abscessus* variant to perform statistical testing, we observed statistically significant increases in the proliferation of *M. abscessus* S compared to R at 7, 14, and 28 dpi (Figure 1B). Furthermore, comparison of the Day 0 and Day 28 burdens demonstrated *M. abscessus* R burdens were statistically unchanged (P>0.99, ANOVA) while *M. abscessus* S burdens increased by approximately 20x across the 4 weeks (P=0.024, ANOVA).

Adult zebrafish mount a robust inflammatory response to *M. abscessus* infection.

The cytokine *tumour necrosis factor* (*tnfa*) is essential for the granulomatous containment of *M. abscessus* in zebrafish embryos (19). To visualize *tnfa* transcription we next took advantage of the *TgBAC(tnfa:GFP)*^{pd1028} zebrafish line (27), where GFP expression is driven by the *tnfa* promoter, to investigate if Tnfa expression is linked to granuloma formation. Expression of GFP was analysed in adult zebrafish infected with either variant of *M. abscessus* at 7, 14, and 28 dpi. GFP was expressed

by host cells in close contact with *M. abscessus* both inside and outside of visibly organised granulomas (Figure 1C).

Granuloma histopathology is accelerated during *M. abscessus* R infection compared to S.

We next performed histology on adult zebrafish infected with fluorescent *M. abscessus* R or S. From 10 dpi we noted a heterogeneous mix of "unorganised lesions" visible as free bacteria around the peritoneal cavity or diffuse foci of bacteria spread throughout host tissue without concentric host nuclear organisation, and "organised granulomas" with stereotypical host nuclei ringing around a central focus of bacteria and the appearance of necrotic cores in all animals (Figure 2A).

We also observed the appearance of very large granulomas filled with fluorescent bacteria and necrotic debris measuring over 500 µm in *M. abscessus* R-infected animals from 14 dpi onwards (Figure 2A). These large granulomas were observed only occasionally and at a rate of no more than 1 per infected animal at 14 and 28 dpi (n=2 with single abscess, 9 without abscess). Three *M. abscessus* R-infected animals were maintained until 70 dpi, all three were found to multiple have granulomas containing fluorescent *M. abscessus* R demonstrating very long lasting infection is possible in adult zebrafish, and two were found to have granulomas measuring over 500 µm suggesting an increase in large granuloma formation with infection duration (Supplemental Figure 1). Granulomas in *M. abscessus* S-infected animals did not reach this size at the 14 and 28 dpi timepoints sampled (n=15 without abscess).

Oil red O staining revealed the accumulation of foam cells in cellular rim of *M. abscessus* R granulomas (Figure 2B), consistent with immunopathology seen in immunocompromised mice infected with *M. abscessus* (15). Conversely, there was little Oil Red O staining in *M. abscessus* S granulomas indicating a lack of foam cell formation (Figure 2C).

We next quantified the number of lesions with the categories of "organised granulomas", with host nuclear organisation into rings, and "unorganised lesions", consisting of either diffuse foci of bacteria spread throughout host tissue or free bacteria around the peritoneal cavity at the whole animal level. The proportion of "organised granulomas" in *M. abscessus* R-infected adult zebrafish from appeared to increase after 10 dpi, however this change was not statistically significant (Figure 3A). *M. abscessus* S was observed to grow freely in mesenteric spaces and form poorly organised cellular granulomas at 14 dpi before the proportion of "organised granulomas" increased at 28 dpi (Figure 3A). The proportion of "organised granulomas" was higher in *M. abscessus* R-infected than

in *M. abscessus* S-infected animals at 14 dpi suggesting granuloma formation is accelerated in R infections compared to S.

These patterns were recapitulated in our quantification of fluorescent bacterial burden in each type of lesion. Significantly more *M. abscessus* R was observed within "organised granulomas" at 14 and 28 dpi than at 10 dpi, and an increase in the proportion of *M. abscessus* S within "organised granulomas" was only observed at 28 dpi compared to 10 and 14 dpi (Figure 3B). The proportion of *M. abscessus* R within "organised granulomas" was higher than the proportion of *M. abscessus* S within "organised granulomas" at 14 dpi, again suggesting accelerated granuloma formation in R variant infections compared to S.

T cell-dependent immunity differentially controls infection by *M. abscessus* variants.

Given the requirement for T cells to maintain granuloma structure in adult zebrafish *M. marinum* infection (25), we next asked if there was T cell involvement around *M. abscessus* granulomas using *TgBAC(lck:EGFP)*^{vcc4} zebrafish (28). We observed T cell association and penetration throughout unorganised and organised *M. abscessus* R granulomas, but T cells were largely excluded from the cores of the very large abscess-like lesions (Figure 4A). We failed to observe T cell interaction with *M. abscessus* S growing "free" around peritoneal organs early in infection, furthermore the T cell response to tissue-invasive *M. abscessus* S was noticeably less than that for equivalent sized *M. abscessus* R granulomas (Figure 4B and Supplemental Figure 2).

To directly test the requirement of T cells in containing *M. abscessus* we next utilised the *lck*$^{-/-sa410}$ mutant line which is T cell-deficient. We infected wild type (WT) control and *lck*$^{-/-sa410}$ mutant adult zebrafish with both the S and R variants. T cell-deficient adult zebrafish were significantly more susceptible to *M. abscessus* R infection with reduced survival over 28 days of infection (P = 0.0005, Log-rank test) (Figure 5A). T cell deficiency had a less pronounced effect on the survival of animals infected with *M. abscessus* S compared to *M. abscessus* R infection (WT S versus lck-/- S P = 0.03, Log-rank test). Within the T cell-deficient animals, there was a 5.5 day increased median survival for *M. abscessus* S-infected animals (34 dpi) compared to *M. abscessus* R (28.5 dpi), although both groups eventually succumbed to infection at the same rate after 35 dpi (P = 0.78, Log-rank test).

Surprisingly, we found necrotic granulomas in a survivor 56 dpi *lck*$^{-/-sa410}$ fish infected with *M. abscessus* R (Supplemental Figure 3). These granulomas were all relatively small compared to the

large granulomas seen in our small sample of 70 dpi WT animals with the largest having necrotic cores of approximately 100 µm.

Bacterial burden was significantly increased in 14 dpi *lck*$^{-/-sa410}$ animals infected with the R, but not the S variant compared to burdens in WT adult zebrafish (Figure 5B). These observations suggest the initial control of *M. abscessus* R infection is more reliant on T cell-mediated immunity than the control *M. abscessus* S infection during the first 2-3 weeks of infection.

The *in vivo* survival advantage of *M. abscessus* S is compromised by *M. abscessus* R in mixed infections.

To further examine our observation that *M. abscessus* S has a survival advantage over *M. abscessus* R in the adult zebrafish infection model, we performed co-infection of adult zebrafish with equal numbers of each variant expressing either Wasabi or tdTomato fluorescent proteins to enable simple tracking (Figure 6A). Coinfection did not affect the recovered *M. abscessus* R burden as near identical *M. abscessus* R CFUs were recovered from single and mixed-infected animals at 7 dpi (Figure 6B). However, coinfection did cause a decrease in the number of recoverable *M. abscessus* S from the levels found in single infections demonstrating a negative effect of R infection on the survival of *M. abscessus* S (Figure 6B). Despite this drop in S burden, analysis of the ratio of recovered R:S colonies revealed a clear and rapid shift in population proportions from 1:1 at 1 dpi to 0.5 rough:1 smooth ratio at 7 dpi that remained stable through to 14 dpi demonstrating partial retention of the relative survival advantage in mixed infection (Figure 6C).

We hypothesised that the T cell response induced by the R variant to antigens shared with the S variant could be responsible for the clearance of S variant in mixed infections. Using our mixed infection animals as individually-controlled experiments, we compared the ratio of R:S colonies at 14 dpi in WT and *lck*$^{-/-sa410}$ zebrafish (Figure 6D). We observed a higher R:S ratio in *lck*$^{-/-sa410}$ zebrafish than in WT zebrafish, suggesting a role for either 1) T cell-dependent immunity in controlling *M. abscessus* R growth or 2) enhanced T cell-independent immunity in suppressing *M. abscessus* S growth.

To distinguish between these two possibilities, we analysed the recovered CFU from WT and T cell-deficient *lck*$^{-/-sa410}$ animals with single and mixed infections of R and S *M. abscessus* at 14 dpi (Figure 6E). CFU recovery from these mixed infections in the T cell-deficient animals revealed a complex interaction between T cell depletion and *M. abscessus* burdens in mixed infections compared to single variant infections. The burden of the R variant *M. abscessus* recovered from

mixed infections was significantly lower than the burdens achieved in single infections, suggesting a T cell-independent effect of the S variant on restraining R growth (P=0.023, 2 way ANOVA). However, there was only a non-statistically significant trend to increased *M. abscessus* R in *lck*$^{-/-sa410}$ mutants compared to WT animals (P=0.99, 2-way ANOVA). Finally, we observed a reduction in the S variant burden recovered from mixed infections compared to single infections in T cell-deficient animals (Figure 6E). However, there was no difference between the recovery of S variant *M. abscessus* in WT or *lck*$^{-/-sa410}$ mutants (P<0.99, 2 way ANOVA), highlighting the complex role of T cells in the R-triggered clearance of S variant *M. abscessus.*

Discussion

In this study, we report for the use of adult zebrafish to probe both host and mycobacterial determinants of pathogenesis during persistent infection with *M. abscessus*. Infection with the R and S variants was maintained at high levels up to one month post infection in genetically intact animals, a major improvement on traditional mouse models of *M. abscessus* infection.

While the R variant induces a more robust and aggressive infection than the S variant in zebrafish embryos (10), this appears to not be the case in the adult fish. We observed better control of R variant burden and establishment of a higher burden of persistent infection with the S variant. One possible explanation for the better survival of the S compared is that infection with the R variant results in earlier granuloma formation and engagement of T cells. This contribution of the T cell response was further substantiated using T cell-deficient fish, where infection of *lck*$^{-/-}$ fish with the R bacilli resulted in a higher bacterial burden than in WT fish at 14 dpi, which was not observed with S bacilli. These observations provide insight into the clinical observation that AIDS patients are not at increased risk of *M. abscessus* infection to the same degree that AIDS is a risk factor for *M. tuberculosis* and other non-tuberculous mycobacterium infections such as *Mycobacterium avium* (29).

It is well known that the intracellular lifestyle of the R and S morphotypes differ significantly, resulting in entirely distinct infection scenarios that, we hypothesise, underlie the accelerated granuloma formation by the R variant in adult zebrafish (30). The absence of GPL on the outer mycomembrane causes corded growth of R variants, resulting in multiple bacilli being simultaneously phagocytosed by macrophages and overloaded phagosomes that rapidly activate autophagy pathways (12, 30). Comparatively, the S variant is able to survive for an extended period of time within the phagosome, producing a chronic and persistent infection (31). As such, these polar infection responses may explain why the R variant displays widespread organised granuloma

277 formation by 14 dpi, compared to S which shows a delayed onset of granuloma formation after 14
278 dpi. Moreover, this observation matches the superior *in vivo* growth performance of S bacilli
279 compared to R, suggesting that the R variant is at an overall disadvantage because of its intrinsic
280 hyper-inflammatory status and the activation of T cell-mediated immunity that appears concomitant
281 with granuloma formation. Interestingly, earlier reports using the zebrafish embryo demonstrated
282 that both bacterial burden and granuloma formation dynamics were similar between both the S and
283 R variants (10, 22), highlighting the critical role of adaptive immunity in divergent *M. abscessus*
284 infection responses. Taken together, our data provide additional evidence for the distinct
285 intracellular fates of both S and R variants *in vivo*, and further implicates the role of adaptive
286 immunity in granuloma formation and control of *M. abscessus* infection in an adult zebrafish
287 model.
288
289 T cells are critical host determinants in the control of mycobacterial infection (29). Recruitment of
290 T cells into granulomas is thought to be essential in containing persistent infection, while T cell
291 deficiencies are associated with greater mycobacterial infection severities (23, 29, 32, 33). Recently,
292 an adult zebrafish infection model for *M. leprae* demonstrated that T cells are essential for
293 containment of infection (23). Herein, we examined the recruitment of T cells within granulomas
294 and identified that S variant granuloma were marked by a relative paucity of T cell infiltration,
295 suggesting that T cells may play a less significant role in S variant infections than those with R
296 variants. Using the *lck*$^{-/-}$ zebrafish, we observed displayed an improved *in vivo* growth performance
297 of the R variant in the absence of T cells when compared to WT animals, highlighting the role of T
298 cells in the control of R variants. This observation was not maintained with the S variant, which
299 showed no increase in bacterial growth *in vivo* irrespective of the absence of T cells early in
300 infection, despite *lck-/-* fish succumbing to intraperitoneal infection within 40 days at the same rate
301 in the absence of T cells irrespective of bacterial morphotype.
302
303 Our co-infection experiments further support the theory that tissue destruction caused by the R
304 variant activates protective trans-acting host immunity that impairs further *M. abscessus* growth.
305 This was seen most clearly in the restriction of *M. abscessus* S growth in mixed infections. It
306 suggests *M. abscessus* must balance the benefits of R variant pathogenicity allowing individuals to
307 kill and escape macrophage containment, with the need to avoid activation of host-protective
308 immunity at a population level when adapting to an animal host. Although we clearly observed an
309 equalisation of this effect in T cell-deficient mutants (Figure 6D), we were unable to determine if
310 this was due to an increase in R growth or suppression of S growth (Figure 6E).
311

The extended maintenance of R variant burden for at least 4 weeks in zebrafish is comparable to our recent data from the C3HeB/FeJ "Kramnik" mouse (34), but the proliferation of S variant up to a log above inoculation dose is unprecedented in a genetically intact vertebrate host. The granulomatous immunopathology in mycobacterium-infected C3HeB/FeJ mice is due to an exaggerated type I interferon response suppressing protective interleukin-1 (35). Further analysis of interferon and interleukin-1 responses to *M. abscessus* infection of mice and zebrafish will help translate our understanding of these dichotomous responses into host directed therapies.

We did not observe switching of S *M. abscessus* into a rough colony morphotype at any timepoint during this or subsequent studies. *In vivo* switching is a rare event that has only been documented in immunocompromised mice or after months-to-years in patients (36, 37). The high S morphotype burdens achieved in adult zebrafish suggest this platform may be useful for future studies of switching during extended infections, with the potential to model responses to chemotherapy.

To date, our understanding of the diverse immune responses between S and R variants have essentially been thoroughly described with respect to innate immunity, and currently our knowledge pertaining to adaptive immunity in *M. abscessus* infection has been poorly characterised (16). Using this new adult zebrafish *M. abscessus* infection model, we have shown that S and R variants produce strikingly different disease phenotypes, which were further exemplified in the absence of T cells. Consequently, these results suggest that the host-pathogen interactions dictating *M. abscessus* pathogenesis are complex and implicate adaptive immunity to a greater extent than originally anticipated. Future work should exploit this relevant animal model in combination with zebrafish lacking the cystic fibrosis transmembrane conductance regulator (CFTR) gene, and for the development and testing of novel antibiotics and vaccine candidates that may be used for the treatment of *M. abscessus* infection.

Methods

Zebrafish strains and handling

Zebrafish strains used in this study are AB strain wildtype, *TgBAC(tnfa:GFP)*^{pd1028}, *TgBAC*(*lck*:*EGFP*)^{vcc4}, *lck-/-* ^{sa410} (27, 28) between 3 and 6 months of age. Animals were held in a 28°C incubator with a 14:10 hour light:dark cycle. Animals were infected by intraperitoneal injection with approximately 10^5 CFU *M. abscessus*, unless otherwise stated, using a 31 G insulin needle and syringe as previously described (38). Infected zebrafish were recovered into system water and held in 1 L beakers with daily feeding for the duration of the experiment. Infection

346 experiments were carried out with ethical approval from the Sydney Local Health District Animal
347 Welfare Committee approval 16-037.
348
349 *M. abscessus* strains and handling
350 Rough (R) and smooth (S) variants of *M. abscessus* strain CIP104536^T were grown at 37°C in
351 Middlebrook 7H9 broth supplemented with 10% Oleic acid/Albumin/Dextrose/Catalase (OADC)
352 enrichment and 0.05% Tween 80 or on Middlebrook 7H10 agar containing 10% OADC (7H10
353 OADC). Recombinant *M. abscessus* strains expressing tdTomato or Wasabi were grown in the
354 presence of 500 µg/ml hygromycin (10, 19). Homogenous bacterial suspensions for intraperitoneal
355 injection in adult fish were prepared as previously reported (39).
356
357 Bacterial recovery
358 Animals were euthanised by tricaine anaesthetic overdose and rinsed in sterile water. Individual
359 carcasses were homogenised and serially diluted into sterile water. Homogenates were plated onto
360 7H10 supplemented with OADC and 300 µg/ml hygromycin. Plates were grown for at least 4 days
361 at 37°C.
362
363 Histology
364 Animals subjected to cryosectioning as previously described (38). Briefly, euthanasia was
365 performed by tricaine anaesthetic overdose and specimens were fixed for 2-4 days in 10% neutral
366 buffered formalin at 4°C. Specimens were then rinsed in PBS, incubated overnight in 30% sucrose,
367 incubated overnight in 50/50 30% sucrose and Tissue-Tek O.C.T. compound (OCT), and finally
368 incubated overnight in OCT prior to freezing at -80°C. Cryosectioning was performed to produce
369 20 µm thick sections. Sections were post-fixed in 10% neutral buffered formalin and rinsed in PBS
370 prior to further processing. Slides for fluorescent imaging were mounted with coverslips using
371 Fluoromount G containing DAPI. Oil Red O staining was performed as previously described (38,
372 40). T cells were detected in sections from *TgBAC(lck:EGFP)*^{vcc4} zebrafish by anti-GFP staining to
373 enhance visible fluorescent green signal (primary antibody: ab13970, Abcam; secondary antibody:
374 ab150173, Abcam), stained slides were then mounted with coverslips using Fluoromount G
375 containing DAPI. All imaging was carried out on a Leica DM6000B microscope.
376
377 Statistics
378 All statistical testing was carried out using Graphpad Prism. Each data point indicates a single
379 animal unless otherwise stated.
380

Acknowledgements

We thank the Centenary imaging facility core and Sydney Cytometry staff Drs Kristina Jahn, Angela Kurz, and David Liu, for their assistance.

Funding: Australian National Health and Medical Research Council CJ Martin Early Career Fellowship APP1053407 and Project Grant APP1099912; The University of Sydney Fellowship G197581; NSW Ministry of Health under the NSW Health Early-Mid Career Fellowships Scheme H18/31086; the Kenyon Family Foundation Inflammation Award; Australian-French Association for Research and Innovation (AFRAN) Initiative; The University of Sydney Marie Bashir Institute 2019 Seed Funding to SHO. Sydney Medical School Summer Scholarship to JYK. Post-doctoral fellowship granted by Labex EpiGenMed, an "Investissements d'avenir" program ANR-10-LABX-12-01 to MDJ; The Fondation pour la Recherche Médicale DEQ20150331719 to LK.

References

1. M. D. Johansen, J. L. Herrmann, L. Kremer, Non-tuberculous mycobacteria and the rise of Mycobacterium abscessus. *Nat Rev Microbiol* 10.1038/s41579-020-0331-1 (2020).
2. H. Medjahed, J. L. Gaillard, J. M. Reyrat, Mycobacterium abscessus: a new player in the mycobacterial field. *Trends Microbiol* **18**, 117-123 (2010).
3. J. F. Tomashefski, Jr., R. C. Stern, C. A. Demko, C. F. Doershuk, Nontuberculous mycobacteria in cystic fibrosis. An autopsy study. *Am J Respir Crit Care Med* **154**, 523-528 (1996).
4. R. Nessar, E. Cambau, J. M. Reyrat, A. Murray, B. Gicquel, Mycobacterium abscessus: a new antibiotic nightmare. *The Journal of antimicrobial chemotherapy* **67**, 810-818 (2012).
5. B. E. Ferro *et al.*, Failure of the Amikacin, Cefoxitin, and Clarithromycin Combination Regimen for Treating Pulmonary Mycobacterium abscessus Infection. *Antimicrob Agents Chemother* **60**, 6374-6376 (2016).
6. S. T. Howard *et al.*, Spontaneous reversion of Mycobacterium abscessus from a smooth to a rough morphotype is associated with reduced expression of glycopeptidolipid and reacquisition of an invasive phenotype. *Microbiology* **152**, 1581-1590 (2006).
7. E. Catherinot *et al.*, Acute respiratory failure involving an R variant of Mycobacterium abscessus. *J Clin Microbiol* **47**, 271-274 (2009).
8. C. R. Esther, Jr., D. A. Esserman, P. Gilligan, A. Kerr, P. G. Noone, Chronic Mycobacterium abscessus infection and lung function decline in cystic fibrosis. *J Cyst Fibros* **9**, 117-123 (2010).

9. B. E. Jonsson *et al.*, Molecular epidemiology of Mycobacterium abscessus, with focus on cystic fibrosis. *J Clin Microbiol* **45**, 1497-1504 (2007).
10. A. Bernut *et al.*, Mycobacterium abscessus cording prevents phagocytosis and promotes abscess formation. *Proc Natl Acad Sci U S A* **111**, E943-952 (2014).
11. H. Medjahed, J. M. Reyrat, Construction of Mycobacterium abscessus defined glycopeptidolipid mutants: comparison of genetic tools. *Appl Environ Microbiol* **75**, 1331-1338 (2009).
12. A. V. Gutierrez, A. Viljoen, E. Ghigo, J. L. Herrmann, L. Kremer, Glycopeptidolipids, a Double-Edged Sword of the Mycobacterium abscessus Complex. *Front Microbiol* **9**, 1145 (2018).
13. A. Bernut, J. L. Herrmann, D. Ordway, L. Kremer, The Diverse Cellular and Animal Models to Decipher the Physiopathological Traits of Mycobacterium abscessus Infection. *Front Cell Infect Microbiol* **7**, 100 (2017).
14. A. Bernut *et al.*, In vivo assessment of drug efficacy against Mycobacterium abscessus using the embryonic zebrafish test system. *Antimicrob Agents Chemother* **58**, 4054-4063 (2014).
15. A. Obregon-Henao *et al.*, Susceptibility of Mycobacterium abscessus to antimycobacterial drugs in preclinical models. *Antimicrob Agents Chemother* **59**, 6904-6912 (2015).
16. M. Rottman *et al.*, Importance of T cells, gamma interferon, and tumor necrosis factor in immune control of the rapid grower Mycobacterium abscessus in C57BL/6 mice. *Infect Immun* **75**, 5898-5907 (2007).
17. C. T. Oh, C. Moon, M. S. Jeong, S. H. Kwon, J. Jang, Drosophila melanogaster model for Mycobacterium abscessus infection. *Microbes Infect* **15**, 788-795 (2013).
18. M. Meir, T. Grosfeld, D. Barkan, Establishment and Validation of Galleria mellonella as a Novel Model Organism To Study Mycobacterium abscessus Infection, Pathogenesis, and Treatment. *Antimicrob Agents Chemother* **62** (2018).
19. A. Bernut *et al.*, Mycobacterium abscessus-Induced Granuloma Formation Is Strictly Dependent on TNF Signaling and Neutrophil Trafficking. *PLoS Pathog* **12**, e1005986 (2016).
20. V. Dubois *et al.*, MmpL8MAB controls Mycobacterium abscessus virulence and production of a previously unknown glycolipid family. *Proc Natl Acad Sci U S A* **115**, E10147-E10156 (2018).
21. I. Halloum *et al.*, Deletion of a dehydratase important for intracellular growth and cording renders rough Mycobacterium abscessus avirulent. *Proc Natl Acad Sci U S A* **113**, E4228-4237 (2016).
22. A. Bernut *et al.*, CFTR Protects against Mycobacterium abscessus Infection by Fine-Tuning Host Oxidative Defenses. *Cell reports* **26**, 1828-1840 e1824 (2019).

23. C. A. Madigan, J. Cameron, L. Ramakrishnan, A Zebrafish Model of Mycobacterium leprae Granulomatous Infection. *J Infect Dis* **216**, 776-779 (2017).
24. S. H. Oehlers *et al.*, Interception of host angiogenic signalling limits mycobacterial growth. *Nature* **517**, 612-615 (2015).
25. L. E. Swaim *et al.*, Mycobacterium marinum infection of adult zebrafish causes caseating granulomatous tuberculosis and is moderated by adaptive immunity. *Infect Immun* **74**, 6108-6117 (2006).
26. M. Parikka *et al.*, Mycobacterium marinum Causes a Latent Infection that Can Be Reactivated by Gamma Irradiation in Adult Zebrafish. *PLoS Pathog* **8**, e1002944 (2012).
27. L. Marjoram *et al.*, Epigenetic control of intestinal barrier function and inflammation in zebrafish. *Proc Natl Acad Sci U S A* **112**, 2770-2775 (2015).
28. K. Sugimoto, S. P. Hui, D. Z. Sheng, M. Nakayama, K. Kikuchi, Zebrafish FOXP3 is required for the maintenance of immune tolerance. *Dev Comp Immunol* **73**, 156-162 (2017).
29. F. M. Collins, Mycobacterial disease, immunosuppression, and acquired immunodeficiency syndrome. *Clin Microbiol Rev* **2**, 360-377 (1989).
30. A.-L. Roux *et al.*, The distinct fate of smooth and rough Mycobacterium abscessus variants inside macrophages. *Open biology* **6** (2016).
31. A. Bernut *et al.*, *Mycobacterium abscessus* cording prevents phagocytosis and promotes abscess formation. *Proceedings of the National Academy of Sciences* **111**, 943-952 (2014).
32. T. Mogues, M. E. Goodrich, L. Ryan, R. LaCourse, R. J. North, The relative importance of T cell subsets in immunity and immunopathology of airborne Mycobacterium tuberculosis infection in mice. *J Exp Med* **193**, 271-280 (2001).
33. J. D. Yang *et al.*, Mycobacterium tuberculosis-specific CD4+ and CD8+ T cells differ in their capacity to recognize infected macrophages. *PLoS Pathog* **14**, e1007060 (2018).
34. V. Le Moigne *et al.*, Efficacy of Bedaquiline, Alone or in Combination with Imipenem, against Mycobacterium abscessus in C3HeB/FeJ Mice. *Antimicrob Agents Chemother* **64** (2020).
35. D. X. Ji *et al.*, Type I interferon-driven susceptibility to Mycobacterium tuberculosis is mediated by IL-1Ra. *Nat Microbiol* **4**, 2128-2135 (2019).
36. I. K. Park *et al.*, Clonal Diversification and Changes in Lipid Traits and Colony Morphology in Mycobacterium abscessus Clinical Isolates. *J Clin Microbiol* **53**, 3438-3447 (2015).
37. A. Pawlik *et al.*, Identification and characterization of the genetic changes responsible for the characteristic smooth-to-rough morphotype alterations of clinically persistent Mycobacterium abscessus. *Mol Microbiol* **90**, 612-629 (2013).

38. T. Cheng, J. Y. Kam, M. D. Johansen, S. H. Oehlers, High content analysis of granuloma histology and neutrophilic inflammation in adult zebrafish infected with Mycobacterium marinum. *Micron* **129**, 102782 (2020).

39. A. Bernut *et al.*, Deciphering and Imaging Pathogenesis and Cording of Mycobacterium abscessus in Zebrafish Embryos. *J Vis Exp* 10.3791/53130 (2015).

40. M. D. Johansen *et al.*, Mycobacterium marinum infection drives foam cell differentiation in zebrafish infection models. *Dev Comp Immunol* **88**, 169-172 (2018).

Figure Legends

Figure 1: *M. abscessus* establishes chronic infection in adult zebrafish.

A. Enumeration of CFUs from adult zebrafish infected with either the R or the S variant of *M. abscessus*. Each point represents a single experimental replicate with at least three animals per timepoint. Total n per timepoint: 0 dpi R=13 S=12; 7 dpi R=18 S=12; 14 dpi R=17 S=13; 28 dpi R=15 S=12.

B. Relative CFUs recovered from adult zebrafish infected with either the R or the S variant of *M. abscessus*. Absolute CFU values were normalised to the inoculum CFU for each experimental replicate. Data is pooled from three replicates per *M. abscessus* variant. Total n per timepoint: 0 dpi R=13 S=12; 7 dpi R=18 S=12; 14 dpi R=17 S=13; 28 dpi R=15 S=12. Statistical tests by T test at each timepoint.

C. Examples of R variant *M. abscessus*-tdTomato lesions in DAPI-stained cryosections from i. 7 dpi, and ii. 14 dpi *TgBAC(tnfa:GFP)*^{pd1028} adult zebrafish. Filled arrowheads indicate organised necrotic granulomas, empty arrowheads indicate loose *M. abscessus* lesions, *tnfa* promoter induction is marked in green.

D. Examples of S variant *M. abscessus*-tdTomato lesions in DAPI-stained cryosections from i. 14 dpi, and ii. 28 dpi *TgBAC(tnfa:GFP)*^{pd1028} adult zebrafish. Filled arrowheads indicate organised granulomas, * indicate necrotic cores, empty arrowheads indicate loose *M. abscessus* lesions, *tnfa* promoter induction is marked in green.

Scale bars indicate 200 μm.

Figure 2: *M. abscessus* infection causes progressive granulomatous pathology.

A. Stereotypical examples of bacterial lesions from DAPI-stained sections from adult zebrafish infected with *M. abscessus* expressing tdTomato. Top row infected with the rough variant, bottom row infected with the smooth variant, timepoint as indicated.

B. Example of Oil Red O-stained very large granuloma in a 14 dpi adult zebrafish infected with R *M. abscessus*. Neutral lipid staining is indicated by red colouration in the macrophages layer surrounding the mycobacterial core, host nuclei are counterstained purple with haematoxylin.

C. Example of Oil Red O-stained large granuloma in 28 dpi adult zebrafish infected with S *M. abscessus*. Note lack of lipid staining in the macrophage rim of the granuloma compared to R granuloma.

Scale bars indicate 200 μm. Filled arrowheads indicate epithelised macrophage nuclei forming a stereotypical concentric layer surrounding the mycobacterial core of organised granulomas, * indicate necrotic cores.

Figure 3: Granuloma histopathology is accelerated during *M. abscessus* R infection compared to S.

A. Quantification of bacterial lesion organisation in adult zebrafish infected with approximately 10^5 CFU *M. abscessus*.

B. Quantification of bacterial burden stratified by lesion organisation in adult zebrafish infected with approximately 10^5 CFU *M. abscessus*.

Total individual lesions analysed (organised/unorganised): 10 dpi R (37/228); 10 dpi S (107/788);14 dpi R (180/314); 14 dpi S (61/352); 28 dpi R (49/93); 28 dpi S (316/476). Statistical testing by ANOVA.

Figure 4: T cell recruitment to S *M. abscessus* infection is delayed compared to R.

A. Examples of T cell recruitment to granulomas in 14 dpi *TgBAC*(*lck*:*EGFP*)^{vcc4} adult zebrafish infected with R *M. abscessus*-tdTomato . i. Example of an unorganised granuloma. ii. Example of a multilobed organised granuloma. iii. Example of a very large granuloma.

B. Example of lack of T cell recruitment to S *M. abscessus*- tdTomato in 14 dpi *TgBAC*(*lck*:*EGFP*)^{vcc4} adult zebrafish. i. Example of *M. abscessus* S mass growing "free" in peritoneal cavity. ii. Example of an unorganised granuloma. iii. Example of an organised granuloma.

Scale bars indicate 100 μm. Filled arrowheads indicate organised granulomas, * indicate necrotic cores, empty arrowheads indicate loose *M. abscessus* lesions, *lck:gfp* positive T cells are marked in green.

Figure 5: T cells are necessary to control R but not S *M. abscessus* infection.

A. Survival analysis of WT and lck$^{-/-\ sa410}$ adult zebrafish infected with R or S *M. abscessus*. Total n=12 WT/*Mabs* R; 16 lck-/-/*Mabs* R; 15 WT/*Mabs* S; 22 lck-/-/*Mabs* S.

552 B. Normalised CFUs recovered from 14 dpi WT and lck$^{-/-\ sa410}$ adult zebrafish infected with *M.*
553 *abscessus*. Each point represents the average of a single experiment with at least 2 animals per
554 group. Total n per group: R WT=12 lck$^{-/-}$=15; S WT=11 lck$^{-/-}$=12. Statistical testing by 2-way
555 ANOVA.
556
557 Figure 6: The *in vivo* survival advantage of *M. abscessus* S is compromised by *M. abscessus* R in
558 mixed infections.
559 A. Schema outlining mixed infection experiment.
560 B. Enumeration of CFUs 7 dpi WT adult zebrafish outlined in panel A. Each point represents the
561 average of a single experiment with at least 2 animals per group. Total n per group: Single R=8,
562 Single S=5, Mixed=5. Statistical testing by 2-way ANOVA.
563 C. Ratio of R:S CFUs recovered from individual WT adult zebrafish from the mixed infection
564 group outlined in panel A.
565 D. Ratio of R:S CFUs recovered from 14 dpi WT and lck$^{-/-\ sa410}$ adult zebrafish infected with a
566 mixture of differentially labelled R and S variants. Statistical testing by Mann-Whitney test.
567 E. Enumeration of CFUs from WT and lck$^{-/-\ sa410}$ adult zebrafish divided into the three groups
568 outlined in panel A. Each point represents the average of a single experimental with at least 3
569 animals per group. Total n per group: WT R=12 S=10 Mixed=10, lck$^{-/-}$ R=9, S=8, Mixed=10.
570 Statistical testing by 2-way ANOVA.
571
572 Supplemental Figure 1
573 Representative images of R *M. abscessus*-tdTomato lesions in DAPI-stained cryosections from
574 three 70 dpi adult zebrafish. Filled arrowheads indicate organised granulomas, * indicate necrotic
575 cores, empty arrowheads indicate loose *M. abscessus* lesions. Scale bars indicate 200 µm.
576
577 Supplemental Figure 2
578 A. Quantification of T cell GFP pixels as a function of *M. abscessus*-tdTomato fluorescence in
579 *TgBAC*(*lck*:*EGFP*)^{vcc4} adult zebrafish. Each point represents the average of a single animal. Total n
580 per group: 14 dpi R=2 S=3, 28 dpi R=3, S=2.
581 B. Quantification of T cell GFP pixels as a function of *M. abscessus*-tdTomato fluorescence in
582 *TgBAC*(*lck*:*EGFP*)^{vcc4} adult zebrafish. Each point represents a single lesion from the animals in
583 Panel A. Total n per group: 14 dpi R=74 S=137, 28 dpi R=91, S=117.
584
585 Supplemental Figure 3

586 Representative images of R *M. abscessus*-tdTomato lesions in DAPI-stained cryosections from a 56
587 dpi *lck*$^{-/-sa410}$ fish. Filled arrowheads indicate organised granulomas, * indicate necrotic cores, empty
588 arrowheads indicate loose *M. abscessus* lesions.

Figure 1

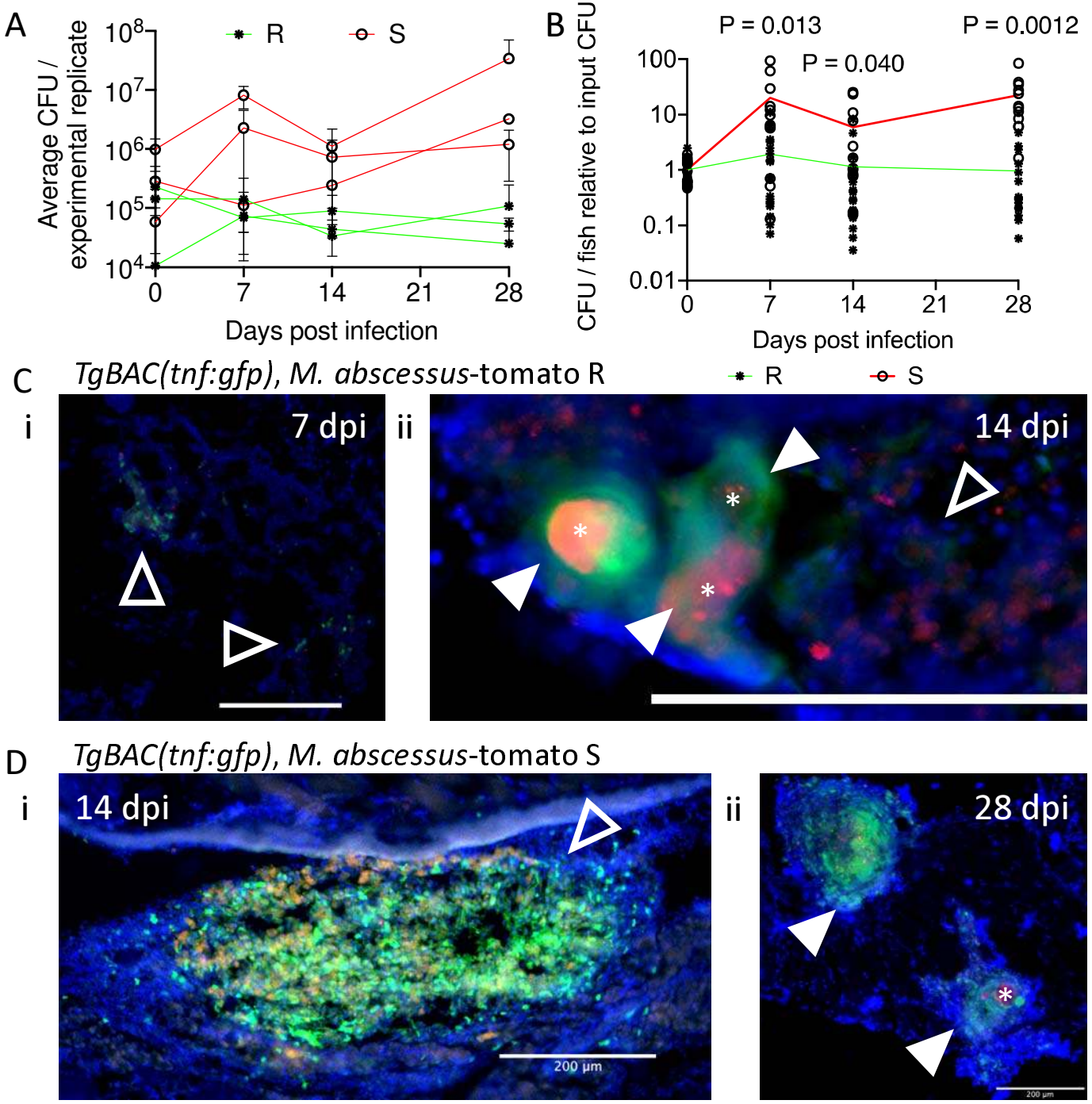

Figure 2

Figure 3

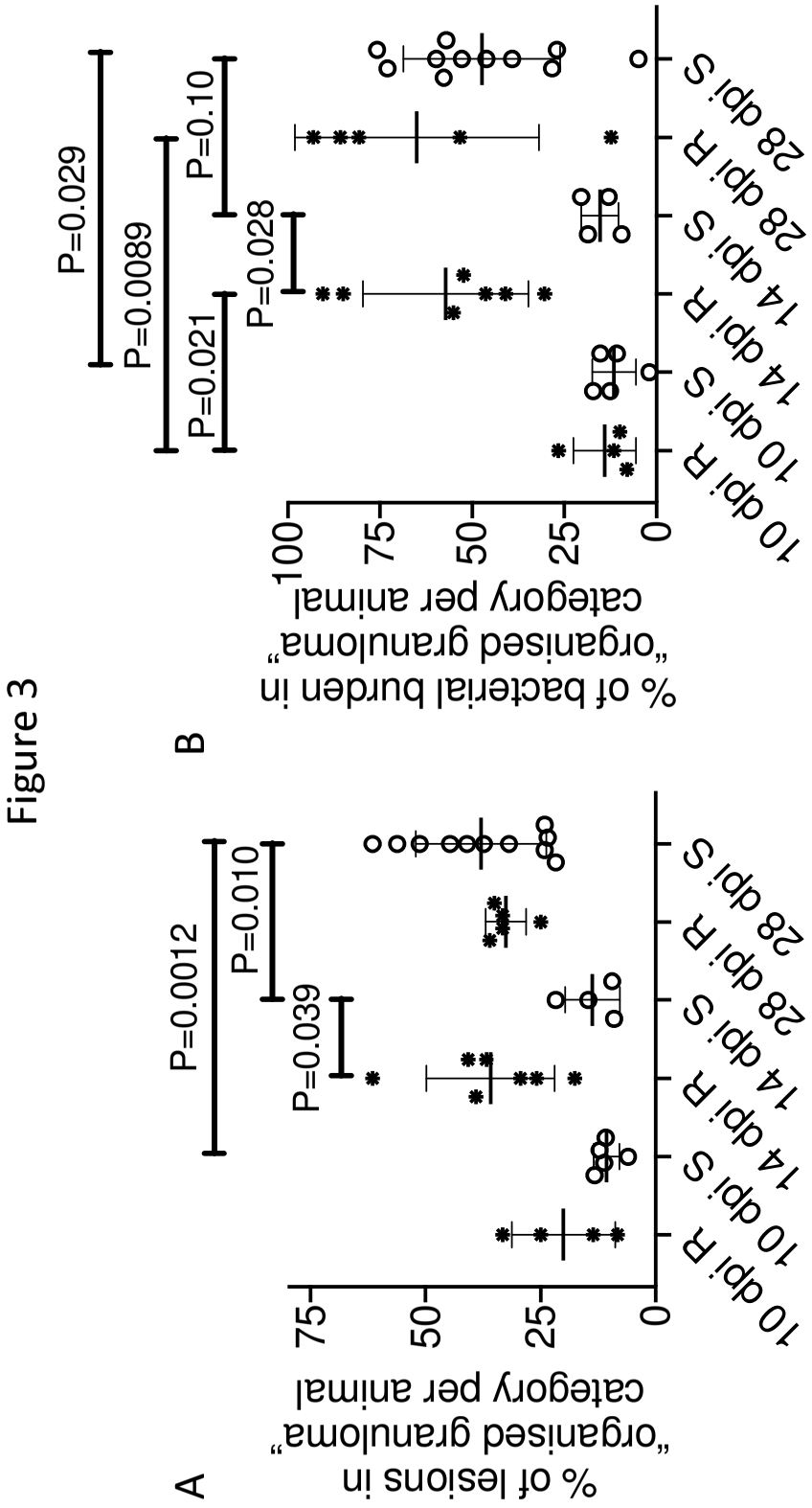

Figure 4

A *TgBAC(lck:gfp), M. abscessus*-Tdtomato Rough variant

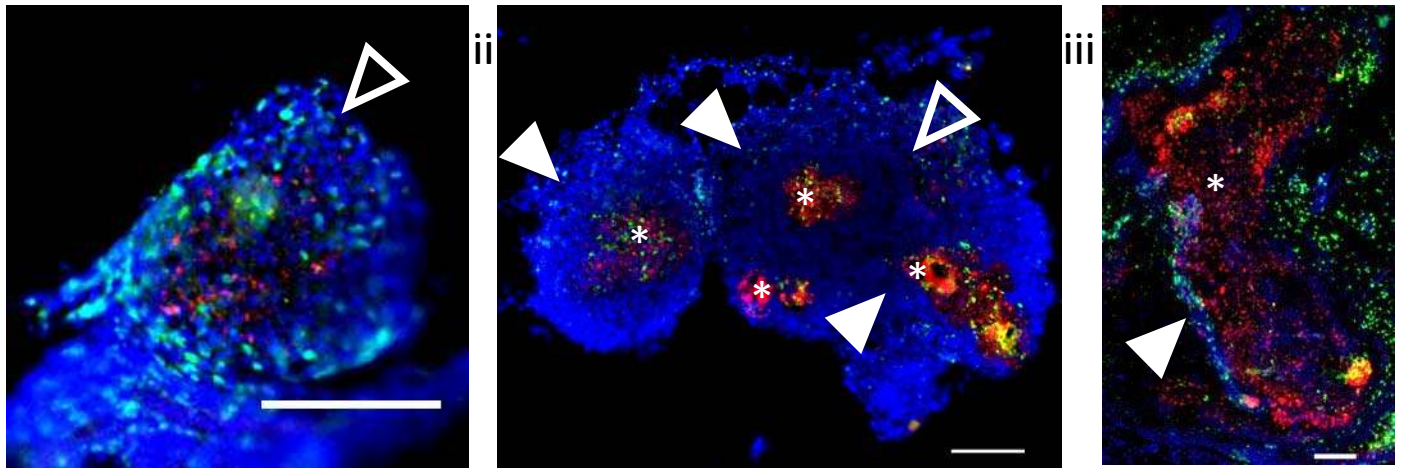

B *TgBAC(lck:gfp), M. abscessus*-Tdtomato Smooth variant

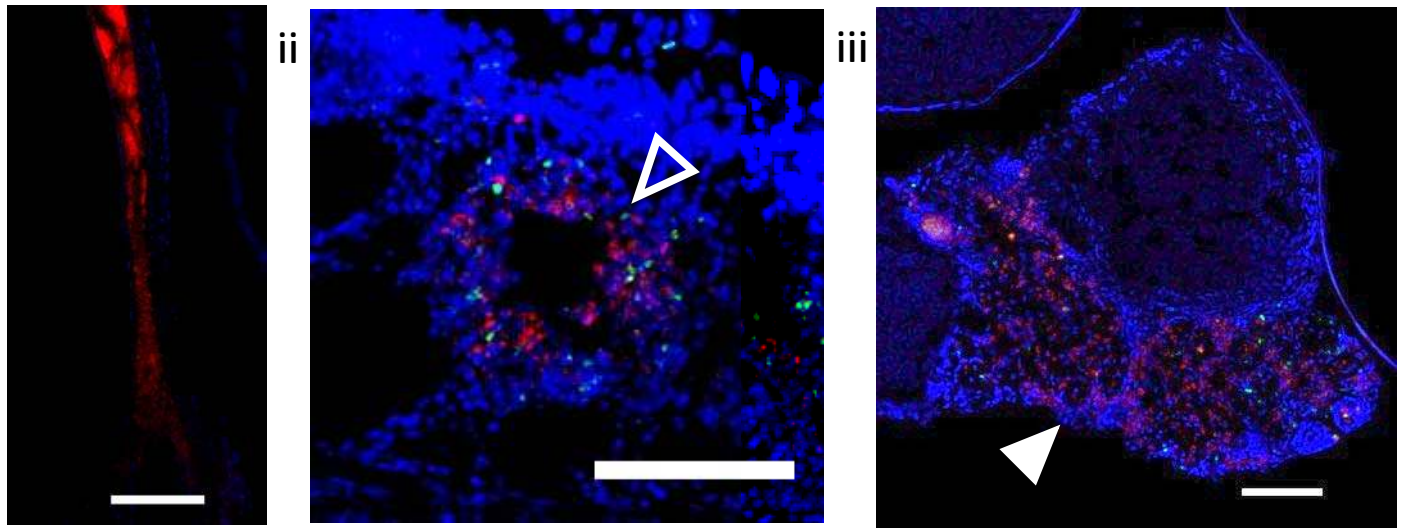

Figure 5

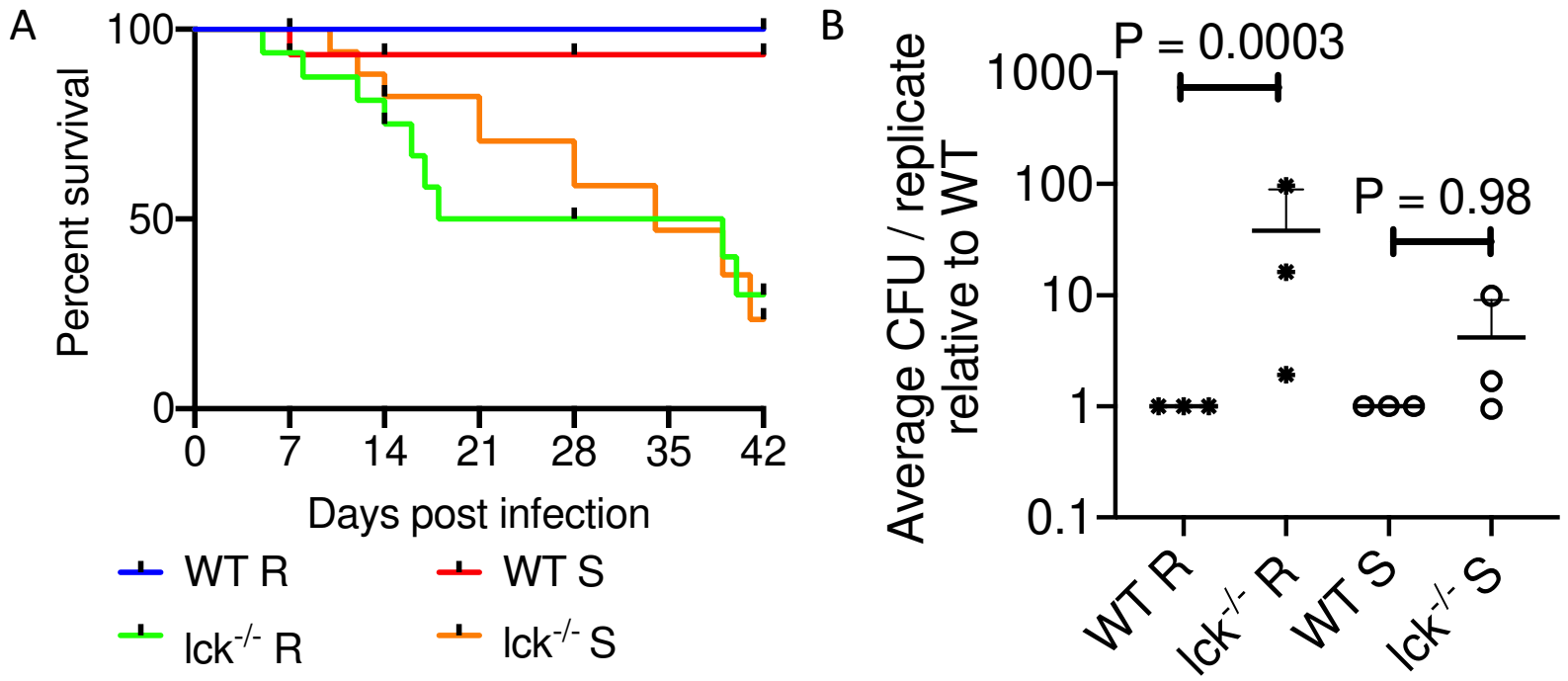

Figure 6

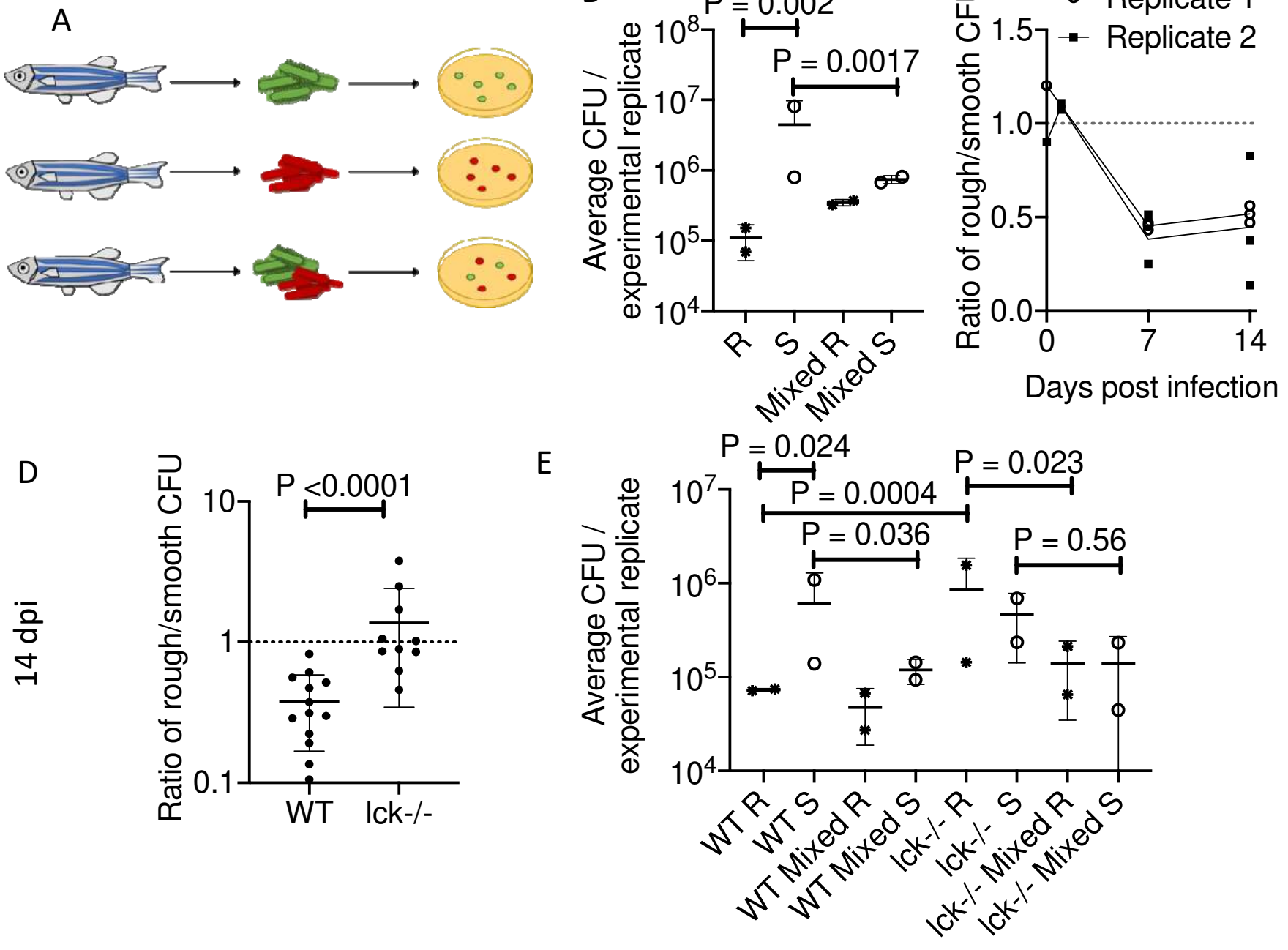

Supplemental Figure 1

Fish 1 of 3 large granuloma

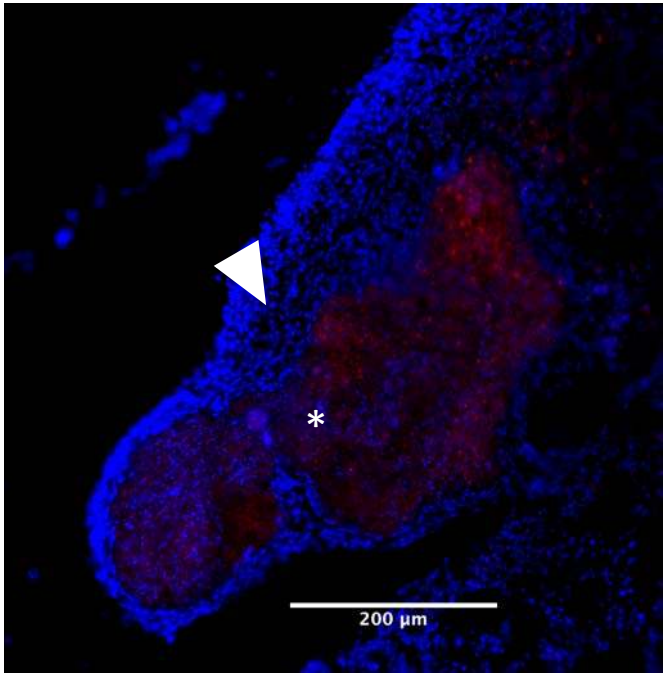

Fish 2 of 3 large granuloma

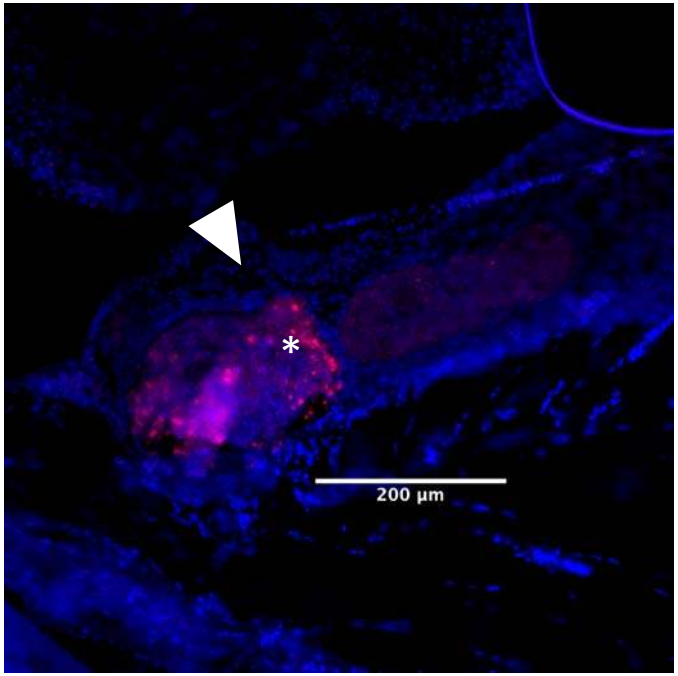

Fish 3 of 3 granuloma clusters

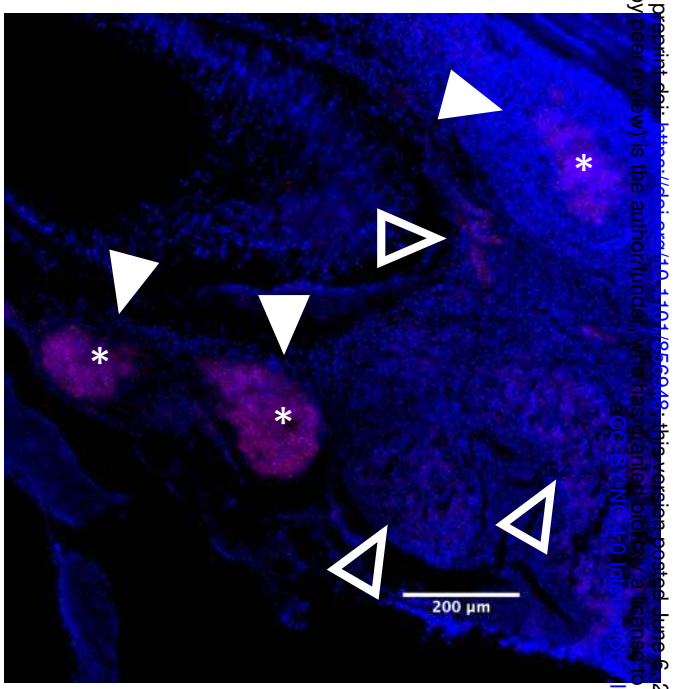

Supplemental Figure 2

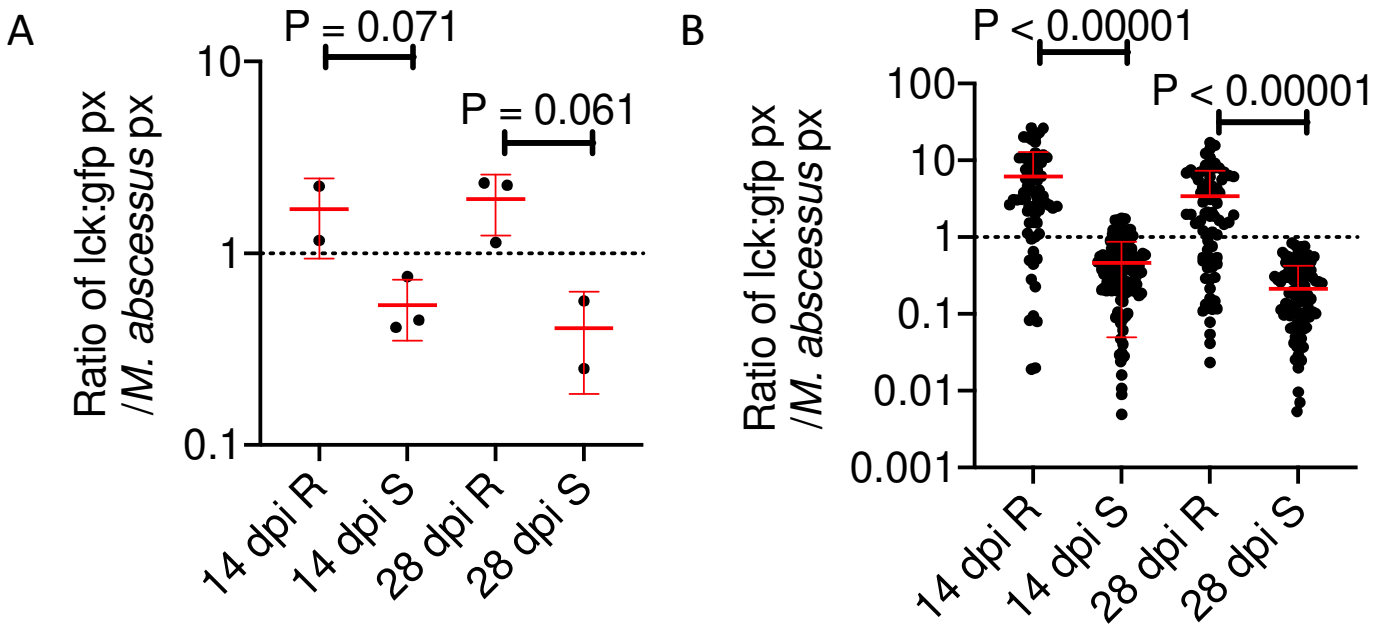

Supplemental Figure 3